

SemanticKITTI: A Dataset for Semantic Scene Understanding of LiDAR Sequences

Jens Behley*

Sven Behnke

Martin Garbade*

Cyrill Stachniss

University of Bonn, Germany

Andres Milioto

Juergen Gall

Jan Quenzel

www.semantic-kitti.org

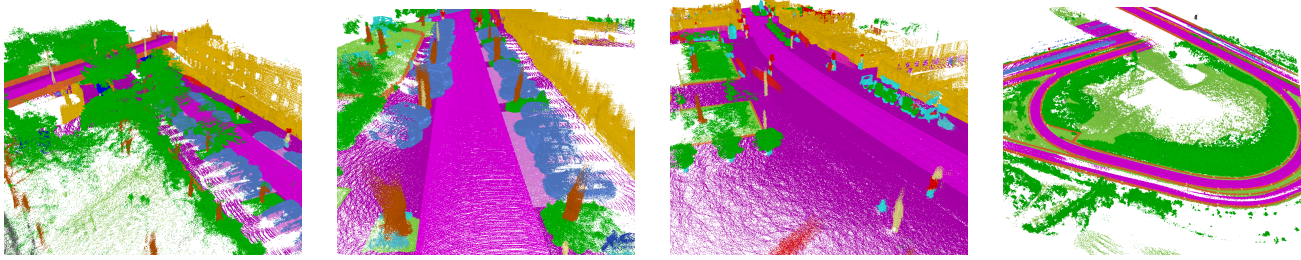


Figure 1: Our dataset provides dense annotations for each scan of all sequences from the KITTI Odometry Benchmark [19]. Here, we show multiple scans aggregated using pose information estimated by a SLAM approach.

Abstract

Semantic scene understanding is important for various applications. In particular, self-driving cars need a fine-grained understanding of the surfaces and objects in their vicinity. Light detection and ranging (LiDAR) provides precise geometric information about the environment and is thus a part of the sensor suites of almost all self-driving cars. Despite the relevance of semantic scene understanding for this application, there is a lack of a large dataset for this task which is based on an automotive LiDAR.

In this paper, we introduce a large dataset to propel research on laser-based semantic segmentation. We annotated all sequences of the KITTI Vision Odometry Benchmark and provide dense point-wise annotations for the complete 360° field-of-view of the employed automotive LiDAR. We propose three benchmark tasks based on this dataset: (i) semantic segmentation of point clouds using a single scan, (ii) semantic segmentation using multiple past scans, and (iii) semantic scene completion, which requires to anticipate the semantic scene in the future. We provide baseline experiments and show that there is a need for more sophisticated models to efficiently tackle these tasks. Our dataset opens the door for the development of more advanced methods, but also provides plentiful data to investigate new research directions.

1. Introduction

Semantic scene understanding is essential for many applications and an integral part of self-driving cars. Particularly, fine-grained understanding provided by semantic segmentation is necessary to distinguish drivable and non-drivable surfaces and to reason about functional properties, like parking areas and sidewalks. Currently, such understanding, represented in so-called high definition maps, is mainly generated in advance using surveying vehicles. However, self-driving cars should also be able to drive in unmapped areas and adapt their behavior if there are changes in the environment.

Most self-driving cars currently use multiple different sensors to perceive the environment. Complementary sensor modalities enable to cope with deficits or failures of particular sensors. Besides cameras, light detection and ranging (LiDAR) sensors are often used as they provide precise distance measurements that are not affected by lighting.

Publicly available datasets and benchmarks are crucial for empirical evaluation of research. They mainly fulfill three purposes: (i) they provide a basis to measure progress, since they allow to provide results that are reproducible and comparable, (ii) they uncover shortcomings of the current state of the art and therefore pave the way for novel approaches and research directions, and (iii) they make it possible to develop approaches without the need to first painstakingly collect and label data. While multiple

* indicates equal contribution

	#scans ¹	#points ²	#classes ³	sensor	annotation	sequential
SemanticKITTI (Ours)	23201/20351	4549	25 (28)	Velodyne HDL-64E	point-wise	✓
Oakland3d [36]	17	1.6	5 (44)	SICK LMS	point-wise	✗
Freiburg [50, 6]	77	1.1	4 (11)	SICK LMS	point-wise	✗
Wachtberg [6]	5	0.4	5 (5)	Velodyne HDL-64E	point-wise	✗
Semantic3d [23]	15/15	4009	8 (8)	Terrestrial Laser Scanner	point-wise	✗
Paris-Lille-3D [47]	3	143	9 (50)	Velodyne HDL-32E	point-wise	✗
Zhang et al. [66]	140/112	32	10 (10)	Velodyne HDL-64E	point-wise	✗
KITTI [19]	7481/7518	1799	3	Velodyne HDL-64E	bounding box	✗

Table 1: Overview of other point cloud datasets with semantic annotations. Ours is by far the largest dataset with sequential information. ¹Number of scans for train and test set, ²Number of points is given in millions, ³Number of classes used for evaluation and number of classes annotated in brackets.

large datasets for *image-based* semantic segmentation exist [10, 39], publicly available datasets with point-wise annotation of three-dimensional point clouds are still comparably small, as shown in Table 1.

To close this gap we propose *SemanticKITTI*, a large dataset showing unprecedented detail in point-wise annotation with 28 classes, which is suited for various tasks. In this paper, we mainly focus on *laser-based* semantic segmentation, but also semantic scene completion. The dataset is distinct from other laser datasets as we provide accurate scan-wise annotations of sequences. Overall, we annotated all 22 sequences of the odometry benchmark of the *KITTI Vision Benchmark* [19] comprised of over 43 000 scans. Moreover, we labeled the complete horizontal 360° field-of-view of the rotating laser sensor. Figure 1 shows example scenes from the provided dataset. In summary, our main contributions are:

- We present a point-wise annotated dataset of point cloud sequences with an unprecedented number of classes and unseen level-of-detail for each scan.
- We furthermore provide an evaluation of state-of-the-art methods for semantic segmentation of point clouds.
- We investigate the usage of sequence information for semantic segmentation using multiple scans.
- Based on the annotation of sequences of a moving car, we furthermore introduce a real-world dataset for semantic scene completion and provide baseline results.
- Together with a benchmark website, the point cloud labeling tool is also publicly available, enabling other researchers to generate other labeled datasets in future.

This large dataset will stimulate the development of novel algorithms, make it possible to investigate new research directions, and puts evaluation and comparison of these novel algorithms on a more solid ground.

2. Related Work

The progress of computer vision has always been driven by benchmarks and datasets [55], but the availability of especially large-scale datasets, such as *ImageNet* [13], was even a crucial prerequisite for the advent of deep learning.

More task-specific datasets geared towards self-driving cars were also proposed. Notable is here the *KITTI Vision Benchmark* [19] since it showed that off-the-shelf solutions are not always suitable for autonomous driving. The *Cityscapes* dataset [10] is the first dataset for self-driving car applications that provides a considerable amount of pixel-wise labeled images suitable for deep learning. The *Mapillary Vistas* dataset [39] surpasses the amount and diversity of labeled data compared to *Cityscapes*.

Also in point cloud-based interpretation, *e.g.*, semantic segmentation, RGB-D based datasets enabled tremendous progress. *ShapeNet* [8] is especially noteworthy for point clouds showing a single object, but such data is not directly transferable to other domains. Specifically, LiDAR sensors usually do not cover objects as densely as an RGB-D sensor due to their lower angular resolution, in particular in vertical direction.

For indoor environments, there are several datasets [48, 46, 24, 3, 11, 35, 32, 12] available, which are mainly recorded using RGB-D cameras or synthetically generated. However, such data shows very different characteristics compared to outdoor environments, which is also caused by the size of the environment, since point clouds captured indoors tend to be much denser due to the range at which objects are scanned. Furthermore, the sensors have different properties regarding sparsity and accuracy. While laser sensors are more precise than RGB-D sensors, they usually only capture a sparse point cloud compared to the latter.

For outdoor environments, datasets were recently proposed that are recorded with a terrestrial laser scanner (TLS), like the *Semantic3d* dataset [23], or using automotive LiDARs, like the *Paris-Lille-3D* dataset [47]. However, the *Paris-Lille-3D* provides only the aggregated scans with

point-wise annotations for 50 classes from which 9 are selected for evaluation. Another recently used large dataset for autonomous driving [57], but with fewer classes, is not publicly available.

The *Virtual KITTI* dataset [17] provides synthetically generated sequential images with depth information and dense pixel-wise annotation. The depth information can also be used to generate point clouds. However, these point clouds do not show the same characteristics as a real rotating LiDAR, including defects like reflections and outliers.

In contrast to these datasets, our dataset combines a large amount of labeled points, a large variety of classes, and sequential scans generated by a commonly employed sensor used in autonomous driving, which is distinct from all publicly available datasets, also shown in Table 1.

3. The SemanticKITTI Dataset

Our dataset is based on the odometry dataset of the KITTI Vision Benchmark [19] showing inner city traffic, residential areas, but also highway scenes and countryside roads around Karlsruhe, Germany. The original odometry dataset consists of 22 sequences, splitting sequences 00 to 10 as training set, and 11 to 21 as test set. For consistency with the original benchmark, we adopt the same division for our training and test set. Moreover, we do not interfere with the original odometry benchmark by providing labels only for the training data. Overall, we provide 23 201 full 3D scans for training and 20 351 for testing, which makes it by a wide margin the largest dataset publicly available.

We decided to use the KITTI dataset as a basis for our labeling effort, since it allowed us to exploit one of the largest available collections of raw point cloud data captured with a car. We furthermore expect that there are also potential synergies between our annotations and the existing benchmarks and this will enable the investigation and evaluation of additional research directions, such as the usage of semantics for laser-based odometry estimation.

Compared to other datasets (cf. Table 1), we provide labels for sequential point clouds generated with a commonly used automotive LiDAR, *i.e.*, the Velodyne HDL-64E. Other publicly available datasets, like *Paris-Lille-3D* [47] or *Wachtberg* [6], also use such sensors, but only provide the aggregated point cloud of the whole acquired sequence or some individual scans of the whole sequence, respectively. Since we provide the individual scans of the whole sequence, one can also investigate how aggregating multiple consecutive scans influences the performance of the semantic segmentation and use the information to recognize moving objects.

We annotated 28 classes, where we ensured a large overlap of classes with the *Mapillary Vistas* dataset [39] and *Cityscapes* dataset [10] and made modifications where nec-

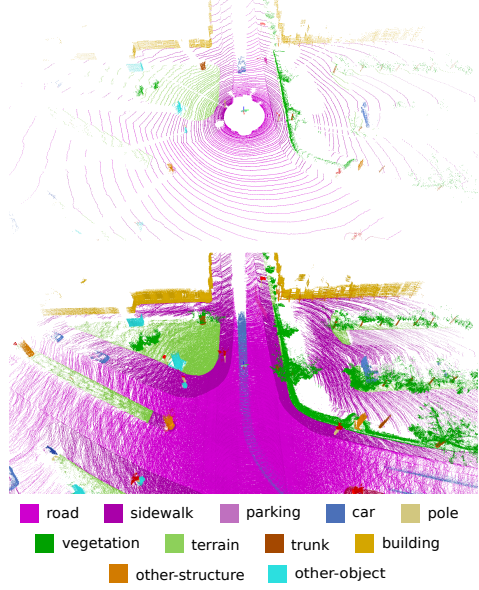


Figure 2: Single scan (top) and multiple superimposed scans with labels (bottom). Also shown is a moving car in the center of the image resulting in a trace of points.

essary to account for the sparsity and vertical field-of-view. More specifically, we do not distinguish between persons riding a vehicle and the vehicle, but label the vehicle and the person as either *bicyclist* or *motorcyclist*.

We furthermore distinguished between moving and non-moving vehicles and humans, *i.e.*, vehicles or humans gets the corresponding moving class if they moved in some scan while observing them, as shown in the lower part of Figure 2. All annotated classes are listed in Figure 3 and a more detailed discussion and definition of the different classes can be found in the supplementary material. In summary, we have 28 classes, where 6 classes are assigned the attribute moving or non-moving, and one *outlier* class is included for erroneous laser measurements caused by reflections or other effects.

The dataset is publicly available through a benchmark website and we provide only the training set with ground truth labels and perform the test set evaluation online. We furthermore will also limit the number of possible test set evaluations to prevent overfitting to the test set [55].

3.1. Labeling Process

To make the labeling of point cloud sequences practical, we superimpose multiple scans above each other, which conversely allows us to label multiple scans consistently. To this end, we first register and loop close the sequences using an off-the-shelf laser-based SLAM system [5]. This step is needed as the provided information of the inertial navigation system (INS) often results in map inconsistencies, *i.e.*, streets that are revisited after some time have differ-

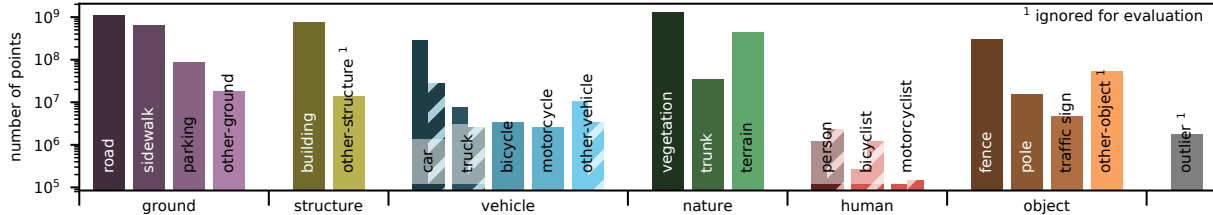


Figure 3: Label distribution. The number of labeled points per class and the root categories for the classes are shown. For movable classes, we also show the number of points on non-moving (solid bars) and moving objects (hatched bars).

ent height. For three sequences, we had to manually add loop closure constraints to get correctly loop closed trajectories, since this is essential to get consistent point clouds for annotation. The loop closed poses allow us to load all overlapping point clouds for specific locations and visualize them together, as depicted in Figure 2.

We subdivide the sequence of point clouds into tiles of 100 m by 100 m. For each tile, we only load scans overlapping with the tile. This enables us to label all scans consistently even when we encounter temporally distant loop closures. To ensure consistency for scans overlapping with more than one tile, we show all points inside each tile and a small boundary overlapping with neighboring tiles. Thus, it is possible to continue labels from a neighboring tile.

Following best practices, we compiled a labeling instruction and provided instructional videos on how to label certain objects, such as cars and bicycles standing near a wall. Compared to image-based annotation, the annotation process with point clouds is more complex, since the annotator often needs to change the viewpoint. An annotator needs on average 4.5 hours per tile, when labeling residential areas corresponding to the most complex encountered scenery, and needs on average 1.5 hours for labeling a highway tile.

We explicitly did not use bounding boxes or other available annotations for the KITTI dataset, since we want to ensure that the labeling is consistent and the point-wise labels should only contain the object itself.

We provided regular feedback to the annotators to improve the quality and accuracy of labels. Nevertheless, a single annotator also verified the labels in a second pass, *i.e.*, corrected inconsistencies and added missing labels. In summary, the whole dataset comprises 518 tiles and over 1 400 hours of labeling effort have been invested with additional 10 – 60 minutes verification and correction per tile, resulting in a total of over 1 700 hours.

3.2. Dataset Statistics

Figure 3 shows the distribution of the different classes, where we also included the root categories as labels on the x-axis. The ground classes, *road*, *sidewalk*, *building*, *vegetation*, and *terrain* are the most frequent classes. The class

motorcyclist only occurs rarely, but still more than 100 000 points are annotated.

The unbalanced count of classes is common for datasets captured in natural environments and some classes will be always under-represented, since they do not occur that often. Thus, an unbalanced class distribution is part of the problem that an approach has to master. Overall, the distribution and relative differences between the classes is quite similar in other datasets, *e.g.* *Cityscapes* [10].

4. Evaluation of Semantic Segmentation

In this section, we provide the evaluation of several state-of-the-art methods for semantic segmentation of a single scan. We also provide experiments exploiting information provided by sequences of multiple scans.

4.1. Single Scan Experiments

Task and Metrics. In semantic segmentation of point clouds, we want to infer the label of each three-dimensional point. Therefore, the input to all evaluated methods is a list of coordinates of the three-dimensional points along with their remission, *i.e.*, the strength of the reflected laser beam which depends on the properties of the surface that was hit. Each method should then output a label for each point of a scan, *i.e.*, one full turn of the rotating LiDAR sensor.

To assess the labeling performance, we rely on the commonly applied mean Jaccard Index or mean intersection-over-union (mIoU) metric [15] over all classes, given by

$$\frac{1}{C} \sum_{c=1}^C \frac{\text{TP}_c}{\text{TP}_c + \text{FP}_c + \text{FN}_c}, \quad (1)$$

where TP_c , FP_c , and FN_c correspond to the number of true positive, false positive, and false negative predictions for class c , and C is the number of classes.

As the classes *other-structure* and *other-object* have either only a few points and are otherwise too diverse with a high intra-class variation, we decided to not include these classes in the evaluation. Thus, we use 25 instead of 28 classes, ignoring *outlier*, *other-structure*, and *other-object* during training and inference.

Furthermore, we cannot expect to distinguish moving from non-moving objects with a single scan, since this Velodyne LiDAR cannot measure velocities like radars exploiting the Doppler effect. We therefore combine the moving classes with the corresponding non-moving class resulting in a total number of 19 classes for training and evaluation.

State of the Art. Semantic segmentation or point-wise classification of point clouds is a long-standing topic [2], which was traditionally solved using a feature extractor, such as Spin Images [29], in combination with a traditional classifier, like support vector machines [1] or even semantic hashing [4]. Many approaches used Conditional Random Fields (CRF) to enforce label consistency of neighboring points [56, 37, 36, 38, 63].

With the advent of deep learning approaches in image-based classification, the whole pipeline of feature extraction and classification has been replaced by end-to-end deep neural networks. Voxel-based methods transforming the point cloud into a voxel-grid and then applying convolutional neural networks (CNN) with 3D convolutions for object classification [34] and semantic segmentation [26] were among the first investigated models, since they allowed to exploit architectures and insights known for images.

To overcome the limitations of the voxel-based representation, such as the exploding memory consumption when the resolution of the voxel grid increases, more recent approaches either upsample voxel-predictions [53] using a CRF or use different representations, like more efficient spatial subdivisions [30, 44, 64, 59, 21], rendered 2D image views [7], graphs [31, 54], splats [51], or even directly the points [41, 40, 25, 22, 43, 28, 14].

Baseline approaches. We provide the results of six state-of-the-art architectures for the semantic segmentation of point clouds in our dataset: PointNet [40], PointNet++ [41], Tangent Convolutions [52], SPLATNet [51], Superpoint Graph [31], and SqueezeSeg (V1 and V2) [60, 61]. Furthermore, we investigate two extensions of SqueezeSeg: DarkNet21Seg and DarkNet53Seg.

PointNet [40] and PointNet++ [41] use the raw unordered point cloud data as input. Core of these approaches is max pooling to get an order-invariant operator that works surprisingly well for semantic segmentation of shapes and several other benchmarks. Due to this nature, however, PointNet fails to capture the spatial relationships between the features. To alleviate this, PointNet++ [41] applies individual PointNets to local neighborhoods and uses a hierarchical approach to combine their outputs. This enables it to build complex hierarchical features that capture both local fine-grained and global contextual information.

Tangent Convolutions [52] also handles unstructured point clouds by applying convolutional neural networks directly on surfaces. This is achieved by assuming that the

data is sampled from smooth surfaces and defining a tangent convolution as a convolution applied to the projection of the local surface at each point into the tangent plane.

SPLATNet [51] takes an approach that is similar to the aforementioned voxelization methods and represents the point clouds in a high-dimensional sparse lattice. As with voxel-based methods, this scales poorly both in computation and in memory cost and therefore they exploit the sparsity of this representation by using bilateral convolutions [27], which only operates on occupied lattice parts.

Similarly to PointNet, Superpoint Graph [31], captures the local relationships by summarizing geometrically homogeneous groups of points into superpoints, which are later embedded by local PointNets. The result is a superpoint graph representation that is more compact and rich than the original point cloud exploiting contextual relationships between the superpoints.

SqueezeSeg [60, 61] also discretizes the point cloud in a way that makes it possible to apply 2D convolutions to the point cloud data exploiting the sensor geometry of a rotating LiDAR. In the case of a rotating LiDAR, all points of a single turn can be projected to an image by using a spherical projection. A fully convolutional neural network is applied and then finally filtered with a CRF to smooth the results. Due to the promising results of SqueezeSeg and the fast training, we investigated how the labeling performance is affected by the number of model parameters. To this end, we used a different backbone based on the Darknet architecture [42] with 21 and 53 layers, and 25 and 50 million parameters respectively. We furthermore eliminated the vertical downsampling used in the architecture.

We modified the available implementations such that the methods could be trained and evaluated on our large-scale dataset. Note that most of these approaches have so far only been evaluated on shape [8] or RGB-D indoor datasets [48]. However, some of the approaches [40, 41] were only possible to run with considerable downsampling to 50 000 points due to memory limitations.

Results and Discussion. Table 2 shows the results of our baseline experiments for various approaches using either directly the point cloud information [40, 41, 51, 52, 31] or a projection of the point cloud [60]. The results show that the current state of the art for point cloud semantic segmentation falls short for the size and complexity of our dataset.

We believe that this is mainly caused by the limited capacity of the used architectures (see Table 9), because the number of parameters of these approaches is much lower than the number of parameters used in leading image-based semantic segmentation networks. As mentioned above, we added DarkNet21Seg and DarkNet53Seg to test this hypothesis and the results show that this simple modification improves the accuracy from 29.5 % for SqueezeSeg to 47.4 % for DarkNet21Seg and to 49.9 % for DarkNet53Seg.

Approach	mIoU	road	sidewalk	parking	other-ground	building	car	truck	bicycle	motorcycle	other-vehicle	vegetation	trunk	terrain	person	bicyclist	motorcyclist	fence	pole	traffic sign
PointNet [40]	14.6	61.6	35.7	15.8	1.4	41.4	46.3	0.1	1.3	0.3	0.8	31.0	4.6	17.6	0.2	0.2	0.0	12.9	2.4	3.7
SPGraph [31]	17.4	45.0	28.5	0.6	0.6	64.3	49.3	0.1	0.2	0.2	0.8	48.9	27.2	24.6	0.3	2.7	0.1	20.8	15.9	0.8
SPLATNet [51]	18.4	64.6	39.1	0.4	0.0	58.3	58.2	0.0	0.0	0.0	0.0	71.1	9.9	19.3	0.0	0.0	0.0	23.1	5.6	0.0
PointNet++ [41]	20.1	72.0	41.8	18.7	5.6	62.3	53.7	0.9	1.9	0.2	0.2	46.5	13.8	30.0	0.9	1.0	0.0	16.9	6.0	8.9
SqueezeSeg [60]	29.5	85.4	54.3	26.9	4.5	57.4	68.8	3.3	16.0	4.1	3.6	60.0	24.3	53.7	12.9	13.1	0.9	29.0	17.5	24.5
SqueezeSegV2 [61]	39.7	88.6	67.6	45.8	17.7	73.7	81.8	13.4	18.5	17.9	14.0	71.8	35.8	60.2	20.1	25.1	3.9	41.1	20.2	36.3
TangentConv [52]	40.9	83.9	63.9	33.4	15.4	83.4	90.8	15.2	2.7	16.5	12.1	79.5	49.3	58.1	23.0	28.4	8.1	49.0	35.8	28.5
DarkNet21Seg	47.4	91.4	74.0	57.0	26.4	81.9	85.4	18.6	26.2	26.5	15.6	77.6	48.4	63.6	31.8	33.6	4.0	52.3	36.0	50.0
DarkNet53Seg	49.9	91.8	74.6	64.8	27.9	84.1	86.4	25.5	24.5	32.7	22.6	78.3	50.1	64.0	36.2	33.6	4.7	55.0	38.9	52.2

Table 2: Single scan results (19 classes) for all baselines on sequences 11 to 21 (test set). All methods were trained on sequences 00 to 10, except for sequence 08 which is used as validation set.

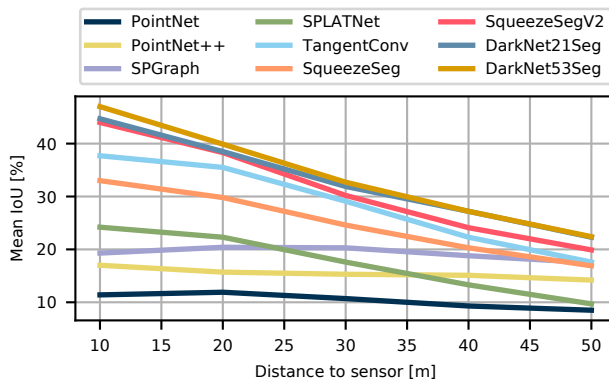


Figure 4: IoU vs. distance to the sensor.

Another reason is that the point clouds generated by LiDAR are relatively sparse, especially as the distance to the sensor increases. This is partially solved in SqueezeSeg, which exploits the way the rotating scanner captures the data to generate a dense range image, where each pixel corresponds roughly to a point in the scan.

These effects are further analyzed in Figure 4, where the mIoU is plotted w.r.t. the distance to the sensor. It shows that results of all approaches get worse with increasing distance. This further confirms our hypothesis that the sparsity is the main reason for worse results at large distances. However, the results also show that some methods, like SPGraph, are less affected by the distance-dependent sparsity and this might be a promising direction for future research to combine the strength of both paradigms.

Especially classes with few examples, like motorcyclists and trucks, seem to be more difficult for all approaches. But also classes with only a small number of points in a single point cloud, like bicycles and poles, are hard classes.

Finally, the best performing approach (DarkNet53Seg) with 49.9% mIoU is still far from achieving results that are on par with image-based approaches, *e.g.*, 80% on the *Cityscapes* benchmark [10].

Approach	num. parameters (million)	train time (GPU hours epoch)	inference time (seconds point cloud)
PointNet	3	4	0.5
PointNet++	6	16	5.9
SPGraph	0.25	6	5.2
TangentConv	0.4	6	3.0
SPLATNet	0.8	8	1.0
SqueezeSeg	1	0.5	0.015
SqueezeSegV2	1	0.6	0.02
DarkNet21Seg	25	2	0.055
DarkNet53Seg	50	3	0.1

Table 3: Approach statistics.

4.2. Multiple Scan Experiments

Task and Metrics. In this task, we allow methods to exploit information from a sequence of multiple past scans to improve the segmentation of the current scan. We furthermore want the methods to distinguish moving and non-moving classes, *i.e.*, all 25 classes must be predicted, since this information should be visible in the temporal information of multiple past scans. The evaluation metric for this task is still the same as in the single scan case, *i.e.*, we evaluate the mean IoU of the current scan no matter how many past scans were used to compute the results.

Baselines. We exploit the sequential information by combining 5 scans into a single, large point cloud, *i.e.*, the current scan at timestamp t and the 4 scans before at timestamps $t-1, \dots, t-4$. We evaluate DarkNet53Seg and TangentConv, since these approaches can deal with a larger number of points without downsampling of the point clouds and could still be trained in a reasonable amount of time.

Results and Discussion. Table 4 shows the per-class results for the movable classes and the mean IoU (mIoU) over all classes. For each method, we show in the upper part of the row the IoU for non-moving (unshaded) and in the lower part of the row the IoU for moving objects (shaded). The

Approach	car	truck	other-vehicle	person	bicyclist	motorcyclist	mIoU
TangentConv [52]	84.9	21.1	18.5	1.6	0.0	0.0	34.1
	40.3	42.2	30.1	6.4	1.1	1.9	
DarkNet53Seg	84.1	20.0	20.7	7.5	0.0	0.0	41.6
	61.5	37.8	28.9	15.2	14.1	0.2	

Table 4: IoU results using a sequence of multiple past scans (in %). Shaded cells correspond to the IoU of the moving classes, while unshaded entries are the non-moving classes.

performance of the remaining static classes is similar to the single scan results and we refer to the supplement for a table containing all classes.

The general trend that the projective methods perform better than the point-based methods is still apparent, which can be also attributed to the larger amount of parameters as in the single scan case. Both approaches show difficulties in separating moving and non-moving objects, which might be caused by our design decision to aggregate multiple scans into a single large point cloud. The results show that especially bicyclist and motorcyclist never get correctly assigned the non-moving class, which is most likely a consequence from the generally sparser object point clouds.

We expect that new approaches could explicitly exploit the sequential information by using multiple input streams to the architecture or even recurrent neural networks to account for the temporal information, which again might open a new line of research.

5. Evaluation of Semantic Scene Completion

After leveraging a sequence of past scans for semantic point cloud segmentation, we now show a scenario that makes use of future scans. Due to its sequential nature, our dataset provides the unique opportunity to be extended for the task of 3D semantic scene completion. Note that this is the first real world outdoor benchmark for this task. Existing point cloud datasets cannot be used to address this task, as they do not allow for aggregating labeled point clouds that are sufficiently dense in both space and time.

In semantic scene completion, one fundamental problem is to obtain ground truth labels for real world datasets. In case of NYUv2 [48] CAD models were fit into the scene [45] using an RGB-D image captured by a Kinect sensor. New approaches often resort to prove their effectiveness on the larger, but synthetic SUNCG dataset [49]. However, a dataset combining the scale of a synthetic dataset and usage of real-world data is still missing.

In the case of our proposed dataset, the car carrying the LiDAR moves past 3D objects in the scene and thereby

records their backsides, which are hidden in the initial scan due to self-occlusion. This is exactly the information needed for semantic scene completion as it contains the full 3D geometry of all objects while their semantics are provided by our dense annotations.

Dataset Generation. By superimposing an exhaustive number of future laser scans in a predefined region in front of the car, we can generate pairs of inputs and targets that correspond to the task of semantic scene completion. As proposed by Song *et al.* [49], our dataset for the scene completion task is a voxelized representation of the 3D scene.

We select a volume of 51.2 m ahead of the car, 25.6 m to every side and 6.4 m in height with a voxel resolution of 0.2 m, which results in a volume of $256 \times 256 \times 32$ voxels to predict. We assign a single label to every voxel based on the majority vote over all labeled points inside a voxel. Voxels that do not contain any points are labeled as *empty*.

To compute which voxels belong to the occluded space, we check for every pose of the car which voxels are visible to the sensor by tracing a ray. Some of the voxels, *e.g.* those inside objects or behind walls are never visible, so we ignore them during training and evaluation.

Overall, we extracted 19 130 pairs of input and target voxel grids for training, 815 for validation and 3 992 for testing. For the test set, we only provide the unlabeled input voxel grid and withhold the target voxel grids. Figure 5 shows an example of an input and target pair.

Task and Metrics. In semantic scene completion, we are interested in predicting the complete scene inside a certain volume from a single initial scan. More specifically, we use as input a voxel grid, where each voxel is marked as empty or occupied, depending on whether or not it contains a laser measurement. For semantic scene completion, one needs to predict whether a voxel is occupied and its semantic label in the completed scene.

For evaluation, we follow the evaluation protocol of Song *et al.* [49] and compute the IoU for the task of scene completion, which only classifies voxel as being occupied or empty, *i.e.*, ignoring the semantic label, as well as mIoU (1) for the task of semantic scene completion over the same 19 classes that were used for the single scan semantic segmentation task (see Section 4).

State of the Art. An early approach addressed the task of scene completion without predicting semantics [16]. This approach was only based on geometric information and therefore did not provide a holistic understanding of the scene. Other approaches tried to fit mesh models to the scene geometry [20]. These approaches, however, are limited by the number of fitted models.

Song *et al.* [49] were the first to address the task of semantic scene completion in an end-to-end fashion. Their work spawned a lot of interest in the field yielding mod-



Figure 5: Left: Visualization of the incomplete input for the semantic scene completion benchmark. Note that we show the labels only for better visualization, but the real input is a single raw voxel grid without any labels. Right: Corresponding target output representing the completed and fully labeled 3D scene.

els that combine the usage of color and depth information [33, 18], address the problem of sparse 3D feature maps by introducing submanifold convolutions [65], increasing the output resolution by deploying a multi-stage coarse to fine training scheme [12]. Other works experimented with new encoder-decoder CNN architectures as well as improving the loss term by adding adversarial loss components [58].

Baseline Approaches. We report the results of three semantic scene completion approaches. First, we apply SSCNet [49] without the flipped TSDF as input feature. This has minimal impact on the performance, but significantly speeds up the training time due to faster preprocessing [18]. Second, we use the Two Stream approach [18], which makes use of the additional information from the RGB image corresponding to the input laser scan. Therefore the RGB image is first processed by a 2D semantic segmentation network, using the approach DeepLab v2 (ResNet-101) [9] trained on Cityscapes to generate a semantic segmentation. The depth information from the single laser scan and the labels inferred from the RGB image are combined in an early fusion. Finally, we modify the Two Stream approach [18] by directly using labels from the best LiDAR-based semantic segmentation approach (DarkNet53Seg).

Results and Discussion. Table 5 shows the results of each of the baselines, whereas results for individual classes are reported in the supplement. The Two Stream network incorporating 2D semantic segmentation of the RGB image outperforms SSCNet which only uses depth information. However, the usage of the best semantic segmentation directly working on the point cloud performs best in this scenario. Nevertheless, the scene completion performance is still low, suggesting the need for further research into more sophisticated models to address this task.

One possible reason for the poor performance is the problem of dealing with the output resolution. SSCNet performs a 4 fold downsampling in a forward pass, followed by a trilinear upsampling to match the target resolution, which renders it incapable of dealing with the details of the scene. Approaches that produce higher output resolutions

	Completion (IoU)	Semantic Scene Completion (mIoU)
SSCNet [49]	76.4	20.7
Two Stream [18]	77.1	21.3
Two Stream [18] + DarkNet53Seg	78.3	24.9

Table 5: Semantic scene completion baselines.

currently fail on our benchmark due to memory limitations. These approaches need some significant adaptation to cope with the desired output resolution and are not ready for off-the-shelf usage. Another challenge for current models is the sparsity of the laser input signal in the far field as can be seen from Figure 5. To obtain a higher resolution input signal in the far field, approaches would have to exploit more efficiently information from high resolution RGB images provided along with each laser scan.

6. Conclusion and Outlook

In this work, we have presented a large-scale dataset showing unprecedented scale in point-wise annotation of point cloud sequences. We provide a range of different baseline experiments for three tasks: (i) semantic segmentation using a single scan, (ii) semantic segmentation using multiple scans, and (iii) semantic scene completion. These experimental results revealed limitations of the baselines, which need to be addressed by the research community.

In future work, we plan to provide also instance-level annotation over the whole sequence, *i.e.*, we want to distinguish different objects in a scan, but also identify the same object over time. This will enable to investigate temporal instance segmentation over sequences. However, we also see potential for other new tasks based on our labeling effort, such as the evaluation of semantic SLAM.

Acknowledgments We thank all students that helped with annotating the data. The work has been funded by the Deutsche Forschungsgemeinschaft (DFG, German Research Foundation) under FOR 1505 Mapping on Demand, BE 5996/1-1, GA 1927/2-2, and under Germanys Excellence Strategy, EXC-2070 – 390732324 (PhenoRob).

References

- [1] A. Agrawal, A. Nakazawa, and H. Takemura. MMM-classification of 3D Range Data. In *Proc. of the IEEE Intl. Conf. on Robotics & Automation (ICRA)*, 2009. 5
- [2] D. Anguelov, B. Taskar, V. Chatalbashev, D. Koller, D. Gupta, G. Heitz, and A. Ng. Discriminative Learning of Markov Random Fields for Segmentation of 3D Scan Data. In *Proc. of the IEEE Conf. on Computer Vision and Pattern Recognition (CVPR)*, pages 169–176, 2005. 5
- [3] I. Armeni, A. Sax, A. Zamir, and S. Savarese. Joint 2D-3D-Semantic Data for Indoor Scene Understanding. *arXiv preprint*, 2017. 2
- [4] J. Behley, K. Kersting, D. Schulz, V. Steinhage, and A. B. Cremers. Learning to Hash Logistic Regression for Fast 3D Scan Point Classification. In *Proc. of the IEEE/RSJ Intl. Conf. on Intelligent Robots and Systems (IROS)*, pages 5960–5965, 2010. 5
- [5] J. Behley and C. Stachniss. Efficient Surfel-Based SLAM using 3D Laser Range Data in Urban Environments. In *Proc. of Robotics: Science and Systems (RSS)*, 2018. 3
- [6] J. Behley, V. Steinhage, and A. Cremers. Performance of Histogram Descriptors for the Classification of 3D Laser Range Data in Urban Environments. In *Proc. of the IEEE Intl. Conf. on Robotics & Automation (ICRA)*, 2012. 2, 3
- [7] A. Boulch, J. Guerry, B. Le Saux, and N. Audebert. SnapNet: 3D point cloud semantic labeling with 2D deep segmentation networks. *Computers & Graphics*, 2017. 5
- [8] A. Chang, T. Funkhouser, L. Guibas, P. Hanrahan, Q. Huang, Z. Li, S. Savarese, M. Savva, S. Song, H. Su, J. Xiao, L. Yi, and F. Yu. ShapeNet: An Information-Rich 3D Model Repository. Technical Report arXiv:1512.03012 [cs.GR], Stanford University and Princeton University and Toyota Technological Institute at Chicago, 2015. 2, 5
- [9] L.-C. Chen, G. Papandreou, I. Kokkinos, K. Murphy, and A. L. Yuille. DeepLab: Semantic image segmentation with deep convolutional nets, atrous convolution, and fully connected crfs. *IEEE Transactions on Pattern Analysis and Machine Intelligence (PAMI)*, 40(4):834–848, 2018. 8, 13
- [10] M. Cordts, M. Omran, S. Ramos, T. Rehfeld, M. Enzweiler, R. Benenson, U. Franke, S. Roth, and B. Schiele. The Cityscapes Dataset for Semantic Urban Scene Understanding. In *Proc. of the IEEE Conf. on Computer Vision and Pattern Recognition (CVPR)*, 2016. 2, 3, 4, 6, 13
- [11] A. Dai, A. X. Chang, M. Savva, M. Halber, T. Funkhouser, and M. Niessner. ScanNet: Richly-annotated 3D Reconstructions of Indoor Scenes. In *Proc. of the IEEE Conf. on Computer Vision and Pattern Recognition (CVPR)*, 2009. 2
- [12] A. Dai, D. Ritchie, M. Bokeloh, S. Reed, J. Sturm, and M. Nießner. ScanComplete: Large-Scale Scene Completion and Semantic Segmentation for 3D Scans. In *Proc. of the IEEE Conf. on Computer Vision and Pattern Recognition (CVPR)*, 2018. 2, 8
- [13] J. Deng, W. Dong, R. Socher, L. Li, K. Li, and L. Fei-Fei. ImageNet: A Large-Scale Hierarchical Image Database. In *Proc. of the IEEE Conf. on Computer Vision and Pattern Recognition (CVPR)*, 2009. 2
- [14] F. Engelmann, T. Kontogianni, J. Schult, and B. Leibe. Know What Your Neighbors Do: 3D Semantic Segmentation of Point Clouds. *arXiv preprint*, 2018. 5
- [15] M. Everingham, S. Eslami, L. van Gool, C. Williams, J. Winn, and A. Zisserman. The Pascal Visual Object Classes Challenge a Retrospective. *International Journal on Computer Vision (IJCV)*, 111(1):98–136, 2015. 4
- [16] M. Firman, O. Mac Aodha, S. Julier, and G. J. Brostow. Structured prediction of unobserved voxels from a single depth image. In *Proc. of the IEEE Conf. on Computer Vision and Pattern Recognition (CVPR)*, pages 5431–5440, 2016. 7
- [17] A. Gaidon, Q. Wang, Y. Cabon, and E. Vig. Virtual Worlds as Proxy for Multi-Object Tracking Analysis. In *Proc. of the IEEE Conf. on Computer Vision and Pattern Recognition (CVPR)*, 2016. 3
- [18] M. Garbade, Y.-T. Chen, J. Sawatzky, and J. Gall. Two Stream 3D Semantic Scene Completion. In *Proc. of the IEEE/CVF Conf. on Computer Vision and Pattern Recognition (CVPR) Workshops*, 2019. 8
- [19] A. Geiger, P. Lenz, and R. Urtasun. Are we ready for Autonomous Driving? The KITTI Vision Benchmark Suite. In *Proc. of the IEEE Conf. on Computer Vision and Pattern Recognition (CVPR)*, pages 3354–3361, 2012. 1, 2, 3, 12
- [20] A. Geiger and C. Wang. Joint 3d object and layout inference from a single rgb-d image. In *Proc. of the German Conf. on Pattern Recognition (GCPR)*, pages 183–195, 2015. 7
- [21] B. Graham, M. Engelcke, and L. van der Maaten. 3D Semantic Segmentation with Submanifold Sparse Convolutional Networks. In *Proc. of the IEEE Conf. on Computer Vision and Pattern Recognition (CVPR)*, 2018. 5
- [22] F. Groh, P. Wieschollek, and H. Lensch. Flex-Convolution (Million-Scale Pointcloud Learning Beyond Grid-Worlds). In *Proc. of the Asian Conf. on Computer Vision (ACCV)*, Dezember 2018. 5
- [23] T. Hackel, N. Savinov, L. Ladicky, J. D. Wegner, K. Schindler, and M. Pollefeys. SEMANTIC3D.NET: A new large-scale point cloud classification benchmark. In *ISPRS Annals of the Photogrammetry, Remote Sensing and Spatial Information Sciences*, volume IV-1-W1, pages 91–98, 2017. 2
- [24] B. Hua, Q. Pham, D. Nguyen, M. Tran, L. Yu, and S. Yeung. SceneNN: A Scene Meshes Dataset with aNNotations. In *Proc. of the Intl. Conf. on 3D Vision (3DV)*, 2016. 2
- [25] B. Hua, M. Tran, and S. Yeung. Pointwise Convolutional Neural Networks. In *Proc. of the IEEE Conf. on Computer Vision and Pattern Recognition (CVPR)*, 2018. 5
- [26] S. Huang. Point Cloud Labeling using 3D Convolutional Neural Network. In *Proc. of the Intl. Conf. on Pattern Recognition (ICPR)*, 2016. 5
- [27] V. Jampani, M. Kiefel, and P. Gehler. Learning Sparse High Dimensional Filters: Image Filtering, Dense CRFs and Bilateral Neural Networks. In *Proc. of the IEEE Conf. on Computer Vision and Pattern Recognition (CVPR)*, 2016. 5
- [28] M. Jiang, Y. Wu, and C. Lu. PointSIFT: A SIFT-like Network Module for 3D Point Cloud Semantic Segmentation. *arXiv preprint*, 2018. 5

- [29] A. Johnson and M. Hebert. Using spin images for efficient object recognition in cluttered 3D scenes. *Trans. on Pattern Analysis and Machine Intelligence (TPAMI)*, 21(5):433–449, 1999. 5
- [30] R. Klukov and V. Lempitsky. Escape from Cells: Deep Kd-Networks for the Recognition of 3D Point Cloud Models. In *Proc. of the IEEE Intl. Conf. on Computer Vision (ICCV)*, 2017. 5
- [31] L. Landrieu and M. Simonovsky. Large-scale Point Cloud Semantic Segmentation with Superpoint Graphs. In *Proc. of the IEEE Conf. on Computer Vision and Pattern Recognition (CVPR)*, 2018. 5, 6, 16
- [32] W. Li, S. Saeedi, J. McCormac, R. Clark, D. Tzoumanikas, Q. Ye, Y. Huang, R. Tang, and S. Leutenegger. InteriorNet: Mega-scale Multi-sensor Photo-realistic Indoor Scenes Dataset. In *Proc. of the British Machine Vision Conference (BMVC)*, 2018. 2
- [33] S. Liu, Y. HU, Y. Zeng, Q. Tang, B. Jin, Y. Han, and X. Li. See and Think: Disentangling Semantic Scene Completion. In *Proc. of the Conf. on Neural Information Processing Systems (NeurIPS)*, pages 261–272, 2018. 8
- [34] D. Maturana and S. Scherer. VoxNet: A 3D Convolutional Neural Network for Real-Time Object Recognition. In *Proc. of the IEEE/RSJ Intl. Conf. on Intelligent Robots and Systems (IROS)*, 2015. 5
- [35] J. McCormac, A. Handa, S. Leutenegger, and A. J. Davison. SceneNet RGB-D: Can 5M Synthetic Images Beat Generic ImageNet Pre-training on Indoor Segmentation? In *Proc. of the IEEE Intl. Conf. on Computer Vision (ICCV)*, 2017. 2
- [36] D. Munoz, J. A. Bagnell, N. Vandapel, and M. Hebert. Contextual Classification with Functional Max-Margin Markov Networks. In *Proc. of the IEEE Conf. on Computer Vision and Pattern Recognition (CVPR)*, 2009. 2, 5
- [37] D. Munoz, N. Vandapel, and M. Hebert. Directional Associative Markov Network for 3-D Point Cloud Classification. In *Proc. of the International Symposium on 3D Data Processing, Visualization and Transmission (3DPVT)*, pages 63–70, 2008. 5
- [38] D. Munoz, N. Vandapel, and M. Hebert. Onboard Contextual Classification of 3-D Point Clouds with Learned High-order Markov Random Fields. In *Proc. of the IEEE Intl. Conf. on Robotics & Automation (ICRA)*, 2009. 5
- [39] G. Neuhold, T. Ollmann, S. R. Bulo, and P. Kortschieder. The Mapillary Vistas Dataset for Semantic Understanding of Street Scenes. In *Proc. of the IEEE Intl. Conf. on Computer Vision (ICCV)*, 2017. 2, 3, 13
- [40] C. Qi, H. Su, K. Mo, and L. Guibas. PointNet: Deep Learning on Point Sets for 3D Classification and Segmentation. In *Proc. of the IEEE Conf. on Computer Vision and Pattern Recognition (CVPR)*, 2017. 5, 6, 13, 16
- [41] C. Qi, L. Yi, H. Su, and L. Guibas. PointNet++: Deep Hierarchical Feature Learning on Point Sets in a Metric Space. In *Proc. of the Conf. on Neural Information Processing Systems (NeurIPS)*, 2017. 5, 6, 13, 16
- [42] J. Redmon and A. Farhadi. YOLOv3: An Incremental Improvement. *arXiv preprint*, 2018. 5
- [43] D. Rethage, J. Wald, J. Sturm, N. Navab, and F. Tombari. Fully-Convolutional Point Networks for Large-Scale Point Clouds. *Proc. of the European Conf. on Computer Vision (ECCV)*, 2018. 5
- [44] G. Riegler, A. Ulusoy, and A. Geiger. OctNet: Learning Deep 3D Representations at High Resolutions. In *Proc. of the IEEE Conf. on Computer Vision and Pattern Recognition (CVPR)*, 2017. 5
- [45] J. Rock, T. Gupta, J. Thorsen, J. Gwak, D. Shin, and D. Hoiem. Completing 3D object shape from one depth image. In *Proc. of the IEEE Conf. on Computer Vision and Pattern Recognition (CVPR)*, 2015. 7
- [46] G. Ros, L. Sellart, J. Materzynska, D. Vazquez, and A. Lopez. The SYNTHIA Dataset: A Large Collection of Synthetic Images for Semantic Segmentation of Urban Scenes. In *Proc. of the IEEE Conf. on Computer Vision and Pattern Recognition (CVPR)*, June 2016. 2
- [47] X. Roynard, J. Deschaud, and F. Goulette. Paris-Lille-3D: A large and high-quality ground-truth urban point cloud dataset for automatic segmentation and classification. *Intl. Journal of Robotics Research (IJRR)*, 37(6):545–557, 2018. 2, 3
- [48] N. Silberman, D. Hoiem, P. Kohli, and R. Fergus. Indoor Segmentation and Support Inference from RGBD Images. In *Proc. of the European Conf. on Computer Vision (ECCV)*, 2012. 2, 5, 7
- [49] S. Song, F. Yu, A. Zeng, A. Chang, M. Savva, and T. Funkhouser. Semantic Scene Completion from a Single Depth Image. In *Proc. of the IEEE Conf. on Computer Vision and Pattern Recognition (CVPR)*, 2017. 7, 8
- [50] B. Steder, G. Grisetti, and W. Burgard. Robust Place Recognition for 3D Range Data based on Point Features. In *Proc. of the IEEE Intl. Conf. on Robotics & Automation (ICRA)*, 2010. 2
- [51] H. Su, V. Jampani, D. Sun, S. Maji, E. Kalogerakis, M.-H. Yang, and J. Kautz. SPLATNet: Sparse Lattice Networks for Point Cloud Processing. In *Proc. of the IEEE Conf. on Computer Vision and Pattern Recognition (CVPR)*, 2018. 5, 6, 13, 16
- [52] M. Tatarchenko, J. Park, V. Koltun, and Q.-Y. Zhou. Tangent Convolutions for Dense Prediction in 3D. In *Proc. of the IEEE Conf. on Computer Vision and Pattern Recognition (CVPR)*, 2018. 5, 6, 7, 16
- [53] L. Tchapmi, C. Choy, I. Armeni, J. Gwak, and S. Savarese. SEGCloud: Semantic Segmentation of 3D Point Clouds. In *Proc. of the Intl. Conf. on 3D Vision (3DV)*, 2017. 5
- [54] G. Te, W. Hu, Z. Guo, and A. Zheng. RGCNN: Regularized Graph CNN for Point Cloud Segmentation. *arXiv preprint*, 2018. 5
- [55] A. Torralba and A. Efros. Unbiased Look at Dataset Bias. In *Proc. of the IEEE Conf. on Computer Vision and Pattern Recognition (CVPR)*, 2011. 2, 3
- [56] R. Triebel, K. Kersting, and W. Burgard. Robust 3D Scan Point Classification using Associative Markov Networks. In *Proc. of the IEEE Intl. Conf. on Robotics & Automation (ICRA)*, pages 2603–2608, 2006. 5
- [57] S. Wang, S. Suo, W. Ma, A. Pokrovsky, and R. Urtasun. Deep Parametric Continuous Convolutional Neural Networks. In *Proc. of the IEEE Conf. on Computer Vision and Pattern Recognition (CVPR)*, 2018. 3

- [58] Y. Wang, D. J. Tan, N. Navab, and F. Tombari. Adversarial Semantic Scene Completion from a Single Depth Image. In *Proc. of the Intl. Conf. on 3D Vision (3DV)*, pages 426–434, 2018. 8
- [59] Z. Wang and F. Lu. VoxSegNet: Volumetric CNNs for Semantic Part Segmentation of 3D Shapes. *arXiv preprint*, 2018. 5
- [60] B. Wu, A. Wan, X. Yue, and K. Keutzer. SqueezeSeg: Convolutional Neural Nets with Recurrent CRF for Real-Time Road-Object Segmentation from 3D LiDAR Point Cloud. In *Proc. of the IEEE Intl. Conf. on Robotics & Automation (ICRA)*, 2018. 5, 6, 13, 16
- [61] B. Wu, X. Zhou, S. Zhao, X. Yue, and K. Keutzer. Squeeze-SegV2: Improved Model Structure and Unsupervised Domain Adaptation for Road-Object Segmentation from a LiDAR Point Cloud. *Proc. of the IEEE Intl. Conf. on Robotics & Automation (ICRA)*, 2019. 5, 6
- [62] J. Xie, M. Kiefel, M. Sun, and A. Geiger. Semantic Instance Annotation of Street Scenes by 3D to 2D Label Transfer. In *Proc. of the IEEE Conf. on Computer Vision and Pattern Recognition (CVPR)*, 2016. 12
- [63] X. Xiong, D. Munoz, J. A. Bagnell, and M. Hebert. 3-D Scene Analysis via Sequenced Predictions over Points and Regions. In *Proc. of the IEEE Intl. Conf. on Robotics & Automation (ICRA)*, pages 2609–2616, 2011. 5
- [64] W. Zeng and T. Gevers. 3DContextNet: K-d Tree Guided Hierarchical Learning of Point Clouds Using Local and Global Contextual Cues. *arXiv preprint*, 2017. 5
- [65] J. Zhang, H. Zhao, A. Yao, Y. Chen, L. Zhang, and H. Liao. Efficient semantic scene completion network with spatial group convolution. In *Proc. of the European Conf. on Computer Vision (ECCV)*, pages 733–749, 2018. 8
- [66] R. Zhang, S. Candra, K. Vetter, and A. Zakhor. Sensor Fusion for Semantic Segmentation of Urban Scenes. In *Proc. of the IEEE Intl. Conf. on Robotics & Automation (ICRA)*, 2015. 2

A. Consistent Labels for LiDAR Sequences

In this section, we explain the implementation of our point cloud labeling tool in more detail and the rationale behind our decision to subdivide the sequences spatially, but not temporally, for getting consistently labeled point cloud sequences. The labeling tool itself was critical to provide the amount of scans with such fine-grained labels.

In summary, we developed an OpenGL-based labeling tool, which exploits parallelization on the GPU. The main challenge is the visualization of vast amounts of point data, but also processing these at the same time, while reaching responsiveness that allows the annotator to label interactively the aggregated point clouds. Figure 6 shows our point cloud annotation program visualizing an aggregated point cloud of over 20 million points. We provide a wide range of tools for annotation, like a brush, a polygon tool, and different filtering methods to hide selected labels. Even with that many points, we are still able to maintain interactive labeling capabilities. Changes to the label of the points inside the aggregated point cloud are reflected in the individual scans, which enables high consistency of the labels over time.

Since we are labeling each point, we are able to annotate objects, even with complex occlusions, more precisely than just using bounding volumes [62]. For instance, we ensured that ground points below a car are labeled accordingly, which was enabled by our filtering capabilities of the annotation tool.

To accelerate the search for points that must be labeled, we used a projective approach to assign labels. To this end, we determine for each point the two-dimensional projection on the screen and then determine for the projection if the point is near to the clicked position (in case of the brush) or inside the selected polygon. Therefore, annotators had to ensure that they did not choose a view that essentially destroyed previously assigned points.

Usually, an annotator performed the following cycle to annotate points: (1) mark points with a specific label and (2) filter points with that label. Due to the filtering of already labeled points, one can resolve occlusions and furthermore ensure that the projective labeling does not destroy already labeled points.

Tile-Based Labeling. An important detail is the aforementioned spatial subdivision of the complete aggregated point cloud into tiles (also shown in the left upper part of Figure 6). Initially, we simply rendered all scans in a range of timestamps, say 100 – 150, and then moved on the next part, say 150 – 200. However, this leads quickly to inconsistencies in the labels, since scans from such parts still overlap and therefore must be relabeled to match labels from before. Since we, furthermore, encounter loop closures with a considerable temporal distance, this overlap can even happen between parts of the sequences that are not temporally close, which even more complicated the task.

Thus, it quickly became apparent that such an additional effort to ensure consistent labels would lead to an unreasonable complicated annotations process and consequently to insufficient results. Therefore, we decided to subdivide the sequence spatially into tiles, where each tile contains all points from scans overlapping with this tile. Consistency at the boundaries between tiles was achieved by having a small overlap between the tiles, which enabled to consistently continue the labels from one tile into another neighboring tile.

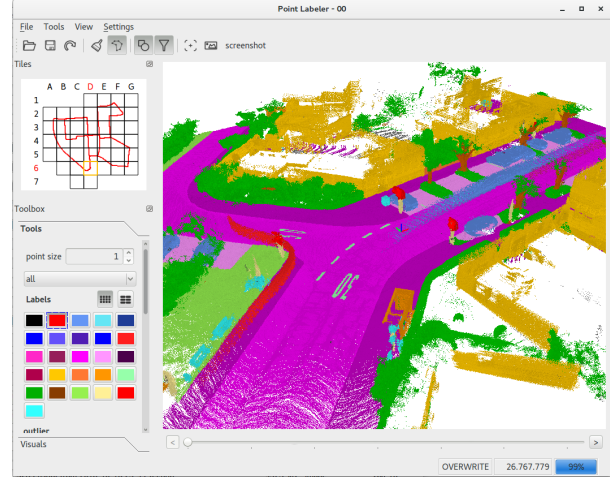


Figure 6: Point cloud labeling tool. In the upper left corner the user sees the tile and the sensor’s path indicated by the red trajectory.

Moving Objects. We annotated all moving objects, i.e., car, truck, person, bicyclist, and motorcyclist, and each moving object is represented by a different class to distinguish it from its corresponding non-moving class. In our case, we assigned an object the corresponding moving class when it moved at some point in time while observing it with the sensor.

Since moving objects will appear at different places when aggregating scans captured from different sensor locations, we had to take special care to annotate moving objects. This is especially challenging, when multiple types of vehicles move on the same lane, like in most of the encountered highway scenes. We annotated moving objects either by filtering ground points or by labeling each scan individually, which was often necessary to label points of tires of a car and bicycles or the feet of persons. But scan-by-scan labeling was also necessary in aforementioned cases where multiple vehicles of different type drive on the same lane. The labeling of moving objects often was the first step when annotating a tile, since this allowed the annotator to filter all moving points and then concentrate on the static parts of the environment.

B. Basis of the Dataset

The basis of our dataset is data from the KITTI Vision Benchmark [19], which is still the largest collection of data also used in autonomous driving at the time of writing. The KITTI dataset is the basis of many experimental evaluations in different contexts and was extended by novel tasks or additional data over time. Thus, we decided to build upon this legacy and also enable synergies between our annotations and other parts and tasks of the KITTI Vision Benchmark.

We particularly decided to use the Odometry Benchmark to enable usage of the annotation data with this task. We expect that exploiting semantic information in the odometry estimation is an interesting avenue for future research. However, also other tasks of the KITTI Vision Benchmark might profit from our annotations

and the pre-trained models we will publish on the dataset website.

Nevertheless, we hope that our effort and the availability of the point labeling tool will enable others to replicate our work on future publicly available datasets from an automotive LiDAR.

C. Class Definition

In the process of labeling such large amounts of data, we had to decide which classes we want to be annotated at some point in time. In general, we followed the class definitions and selection of the *Mapillary Vistas* dataset [39] and *Cityscapes* [10] dataset, but did some simplifications and adjustments for the data source used.

First, we do not explicitly consider a *rider* class for persons riding a motorcycle or a bicycle, since the available point clouds do not provide the density for a single scan to distinguish the person riding a vehicle. Furthermore, we get for such classes only moving examples and therefore cannot easily aggregate the point clouds to increase the fidelity of the point cloud and make it easier to distinguish the rider of a vehicle and the vehicle.

We furthermore had to keep the class selection fixed, even though we encountered while labeling situation where we thought that adding a class would have been beneficial. In particular, the classes *other-structure*, *other-vehicle*, and *other-object* are fallback classes of their respective root category in unclear cases or missing classes, since this simplified the labeling process and might be used to distinguish these categories further in future.

Annotators often annotated some object or part of the scene and then hide the labeled points to avoid overwriting or removing the labels. Thus, assigning the fallback class in ambiguous cases or cases where a specific class was missing made it possible to simply hide that class to avoid overwriting it. If we had instructed the annotators to label such parts as unlabeled, it would have caused problems to consistently label the point clouds.

For the vehicle category (except bicycle and motorcycle, since we assume that these cannot move without a human) and human category, we additionally distinguished between non-moving and moving, *i.e.*, it moved while observing the object. We furthermore distinguished between moving and non-moving vehicles and humans, *i.e.*, a vehicle gets the moving vehicle class if it moved in some scan while observing the vehicle.

In summary, we annotated 28 classes and all annotated classes with their respective definitions are listed in Table 6 on the next page.

D. Baseline Setup

We modified the available implementations such that the methods could be trained and evaluated on our large-scale dataset with very sparse point clouds due to the LiDAR sensor. Note that most of these approaches have so far only been evaluated on small RGB-D indoor datasets.

We restricted the number of points within a single scan due to memory limitations on some approaches [40, 41] to 50 000 via random sampling.

For SPLATNet, we used the SPLATNet_{3D}¹ architecture from [51]. The input consisted per point of the 3D position and its

normal. The normals were previously estimated given 30 closest neighbors.

With TangentConv² we used the existing configuration for Semantic3D. We sped up the training and validation procedures by precomputing scan batches and added asynchronous data loading. Complete single scans were provided during training. In the multi scan experiment we fixed the number of points per batch to 500 000 due to memory constraints and started training from the single scan weights.

For SqueezeSeg [60] and its Darknet backbone equivalents, we used a spherical projection of the scans in the same way as the original SqueezeSeg approach. The projection contains 64 lines in height corresponding with the separate beams of the sensor, and extrapolating the configuration of SqueezeSeg which only uses the front 90° and a horizontal resolution of 512, we use 2048 for the entire scan. Because some points are duplicated in this sampling process, we always keep the closest range value, and in inference of each scan we iterate over the entire point list and check it's semantic value in the output grid.

An overview of the used parameters is given in Table 9. We furthermore provide the number of trained epochs and if we could get a results which seems to be converged in the given amount of time.

E. Results using Multiple Scans

The full per class IoU results for the multiple scans experiment are listed in Table 7. As already mentioned in the main text, we generally observe that the IoU of static classes is mostly unaffected by the availability of multiple past scans. To some extent, the IoU for some classes increases slightly. The drop in performance in terms of mIoU is mainly caused by the additional challenge to correctly separate moving and non-moving classes.

F. Semantic Scene Completion

Table 8 shows the class-wise results for semantic scene completion as well as precision and recall for scene completion. The best approach with respect to semantic scene completion (Two Stream [?] + DarkNet53Seg) outperforms the other two approaches significantly on the classes traffic sign (+14.4 %), parking (+8.3 %), car (+7.7 %), terrain (7.6 %), and other vehicle (5.1 %). Note that DarkNet53Seg has been pretrained on the exact same classes as required for semantic scene completion. Two Stream on the other hand uses DeepLab v2 (ResNet-101) [9] pretrained on the Cityscapes [10] dataset, which does not differentiate between classes such as other-ground, parking or trunk for example. Another reason might be that 2D semantic labels projected back onto the point cloud is not very accurate especially at object boundaries, where labels often bleed onto distant objects. This is because in the 2D projection, they are close to each other, a problem that is inherent to the projection method. Rare classes like bicycle, motorcycle, motorcyclist, and person are not or almost not recognized. This suggests that these classes are potentially hard to recognize, as they represent a small and rare signal in the SemanticKITTI data.

¹<https://github.com/NVlabs/splatnet>

²https://github.com/tatarchm/tangent_conv

cat. class	definition
Ground-related	road Drivable areas where cars are allowed to drive on including service lanes, bike lanes, crossed areas on the street. Only the road surface is labeled excluding the curb.
	sidewalk Areas used mainly by pedestrians, bicycles, but not meant for driving with a car. This includes curbs and spaces where you are not allowed to drive faster than 5 km h^{-1} . Private driveways are also labeled as sidewalk. Here cars should also not drive with regular speeds (such as 30 or 50 km h^{-1}).
	parking Areas meant explicitly for parking and that are clearly separated from sidewalk and road by means of a small curb. If unclear then <i>other-ground</i> or <i>sidewalk</i> can be selected. Garages are labeled as <i>building</i> and not as parking.
	other-ground This label is chosen whenever a distinction between sidewalk and terrain is unclear. It includes (paved/plastered) traffic islands which are not meant for walking. Also the paved parts of a gas station are not meant for parking.
structures	building The whole building including building walls, doors, windows, stairs, etc. Garages count as building.
	other-structure This includes other vertical structures, like tunnel walls, bridge posts, scaffolding on a building from a construction site or bus stops with a roof.
vehicle	car Cars, jeeps, SUVs, vans with a continuous body shape (i.e. the driver cabin and cargo compartment are one) are included.
	truck Trucks, vans with a body that is separate from the driver cabin, pickup trucks, as well as their attached trailers.
	bicycle Bicycles without the cyclist or possibly other passengers. If the bicycle is driven by a person or a person stands nearby the vehicle, we label it as bicyclist.
	motorcycle Motorcycles, mopeds without the driver or other passengers. Includes also motorcycles covered by a cover. If the motorcycle is driven by a person or a person stands nearby the vehicle, we label it as motorcyclist.
	other-vehicle Caravans, Trailers and fallback category for vehicles not explicitly defined otherwise in the meta category <i>vehicle</i> . Included are buses intended for 9+ persons for public or long-distance transport. This further includes all vehicles moving on rails, e.g., trams, trains.
nature	vegetation Vegetation are all bushes, shrubs, foliage, and other clearly identifiable vegetation.
	trunk The tree trunk is labeled as <i>trunk</i> separately from the treetop which gets the label <i>vegetation</i> .
	terrain Grass and all other types of horizontal spreading vegetation, including soil.
human	person Humans moving by their own legs, sitting, or any unusual pose, but not meant to drive a vehicle.
	bicyclist Humans driving a bicycle or standing in close range to a bicycle (within <i>arm reach</i>). We do not distinguish between riders and bicyclist.
	motorcyclist Humans driving a motorcycle or standing in close range to a motorcycle (within <i>arm reach</i>).
object	fence Separators, like fences, small walls and crash barriers.
	pole Lamp posts and the poles of traffic signs.
	traffic sign Traffic sign excluding its mounting. Spurious points in a layer in front and behind the traffic sign are also labeled as traffic sign and not as outlier.
	other-object Fallback category that includes advertising columns.
outlier	outlier Outlier are caused by reflections or inaccuracies in the deskewing of scans, where it is unclear where the points came from.

Table 6: Class definitions.

Approach	road	sidewalk	parking	other-ground	building	car	car (moving)	truck	truck (moving)	bicycle	motorcycle	other-vehicle	other-vehicle (moving)	vegetation	trunk	terrain	person	person (moving)	bicyclist	motorcyclist	fence	pole	traffic-sign	mIoU		
TangentConv	83.9	64.0	38.3	15.3	85.8	84.9	40.3	21.1	42.2	2.0	18.2	18.5	30.1	79.5	43.2	56.7	1.6	6.4	0.0	1.1	0.0	1.9	49.1	36.4	31.2	34.1
DarkNet53Seg	91.6	75.3	64.9	27.5	85.2	84.1	61.5	20.0	37.8	30.4	32.9	20.7	28.9	78.4	50.7	64.8	7.5	15.2	0.0	14.1	0.0	0.2	56.5	38.1	53.3	41.6

Table 7: IoU results using a sequence of multiple past scans (in %).

Approach	Scene Completion			Semantic Scene Completion																				mIoU
	precision	recall	IoU	road	sidewalk	parking	other-ground	building	car	truck	bicycle	motorcycle	other-vehicle	vegetation	trunk	terrain	person	person (moving)	bicyclist	motorcyclist	fence	pole	traffic sign	
SSCNet	90.2	83.4	76.4	67.9	36.5	24.5	8.7	51.7	42.0	3.3	0.0	0.0	0.1	55.1	23.5	30.9	0.0	0.0	0.0	24.8	18.4	6.3	20.7	
Two Stream	90.1	84.2	77.1	68.4	37.6	25.5	7.3	54.3	40.5	7.9	0.0	0.0	0.2	56.9	22.0	34.6	0.0	0.1	0.0	22.0	18.3	8.1	21.3	
Two Stream + DarkNet53Seg	87.4	88.3	78.3	72.3	43.0	33.8	8.0	55.1	48.2	4.1	0.1	0.0	5.3	56.5	25.6	42.2	3.2	2.3	0.0	29.1	21.9	22.5	24.9	

Table 8: Results for scene completion and class-wise results for semantic scene completion (in %).

Approach	scan size	projected	learning rate	epochs trained	converged
PointNet	50 000	-	$3 \cdot 10^{-4} \times 0.9$ epoch	33	✓
PointNet++	45 000	-	$3 \cdot 10^{-3} \times 0.9$ epoch	25	✓
TangentConv	120 000	-	$1 \cdot 10^{-4}$	10	✓
SPLATNet	50 000	-	$1 \cdot 10^{-3}$	20	-
SqueezeSeg	64 × 2048	✓	$1 \cdot 10^{-2} \times 0.99$ epoch	200	✓
DarkNet21Seg	64 × 2048	✓	$1 \cdot 10^{-3} \times 0.99$ epoch	40	✓
DarkNet53Seg	64 × 2048	✓	$1 \cdot 10^{-3} \times 0.99$ epoch	120	✓
TangentConv	500 000	-	5^*	✓	
DarkNet53Seg64	64 × 2048	✓	$1 \cdot 10^{-3} \times 0.99$ epoch	40*	✓

Table 9: Approach statistics. * in number of epochs means that it was started from the pretrained weights of the single scan version.

G. Qualitative Results

Figure 7 shows qualitative results for the evaluated base line approach on a scan from the validation data. Here we show the spherical projections of the results to enable an easier comparison of the results.

With increasing performance in terms of mean IoU (top to bottom), see also Table 2 of the paper, we see that ground points get better separated into the classes sidewalk, road, and parking. In particular, parking areas need a lot of contextual information and also information from neighboring points, since often a small curb distinguishes the parking area from the road.

In general, one can see definitely an increased accuracy for smaller objects like the poles on the right side of the image, which indicates that the extra parameters of the models with the largest capacity (25 million as in the case of DarkNet21Seg and 50 million as in the case of Darknet53Seg) are needed to distinguish smaller classes and class with few examples.

H. Dataset and Baseline Access API

Along with the annotations and the labeling tool, we also provide a public API implemented in Python.

In contrast with our labeling tool which is intended at allowing users to easily extend this dataset, and generate others for other purposes, this API is intended to be used to easily access the data, calculate statistics, evaluate metrics, and access several implementations of different state-of-the-art semantic segmentation approaches. We hope that this API will serve as a baseline to implement new point cloud semantic segmentation approaches, and will provide a common framework to evaluate them, and compare them more transparently with other methods. The choice of Python as the underlying language for the API is that it is the current language of choice for the front end for deep learning framework developers, and therefore, for deep learning practitioners.

Figure 8 gives an overview of the labeled sequences showing the estimated trajectories and the aggregated point cloud over the whole sequence.



Figure 7: Examples of inference for all methods. The point clouds were projected to 2D using a spherical projection to make the comparison easier.

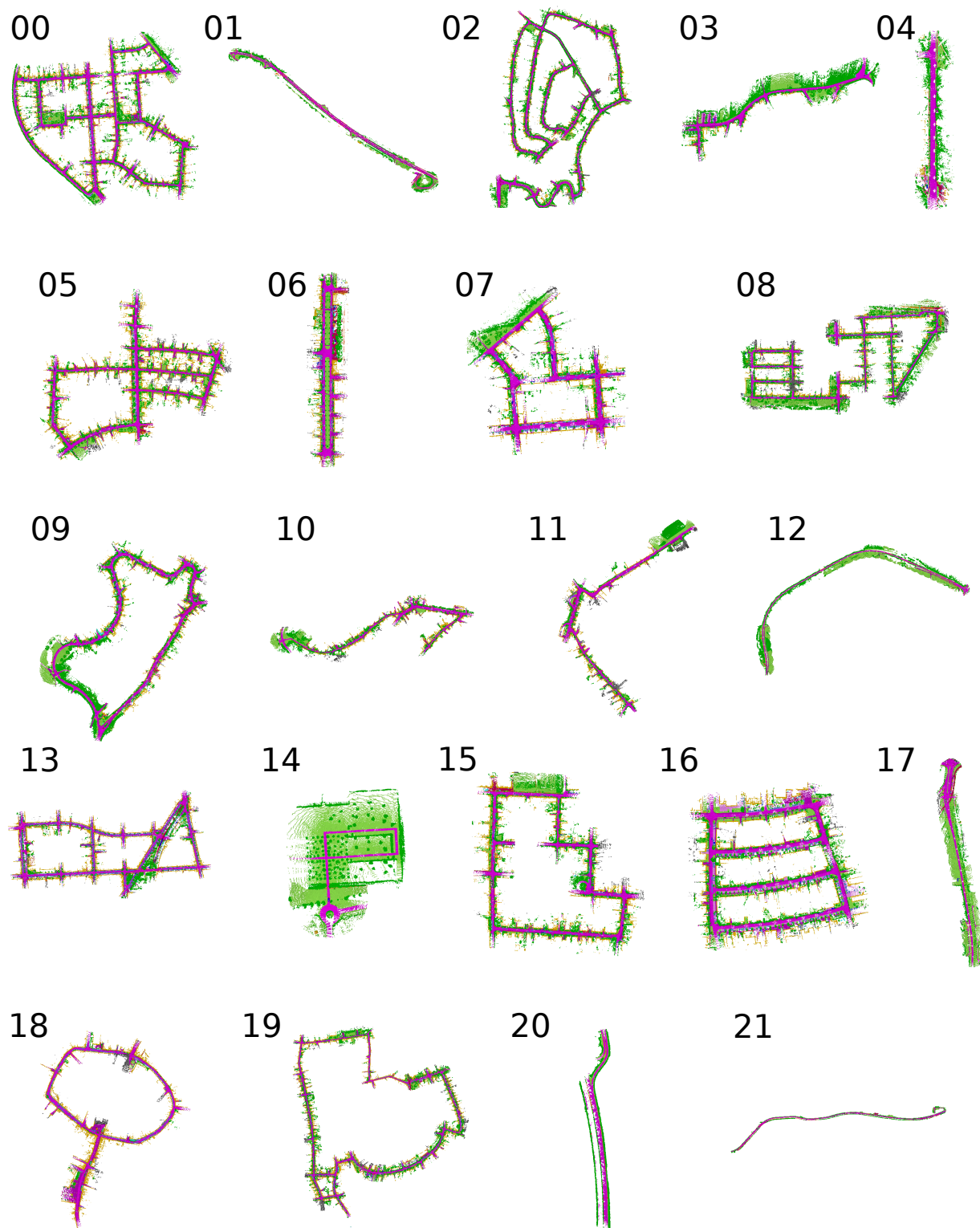


Figure 8: Qualitative overview of labeled sequences and trajectories.